International Journal of Computer Assisted Radiology and Surgery
https://doi.org/10.1007/s11548-021-02527-6

ORIGINAL ARTICLE

Automatic detection of attachment sites for knee ligaments and tendons on CT images

Alexandra Yurova[1] · Victoria Salamatova[1,2] · Alexey Lychagin[1] · Yuri Vassilevski[1,2]

Received: 6 June 2021 / Accepted: 20 October 2021

Abstract

Purpose The diseases and injuries of the knee joint are the most common orthopedic disorders. Personalized knee models can be helpful in the process of early intervention and lasting treatment techniques development. Fully automatic reconstruction of knee joint anatomical structures from medical images (CT, MRI, ultrasound) remains a challenge. For this reason, most of state-of-the-art knee joint models contain simplifications such as representation of muscles and ligaments as line segments connecting two points which replace attachment areas. The paper presents algorithms for automatic detection of such points on knee CT images.

Methods This paper presents three approaches to automatic detection of ligaments and tendons attachment sites on the patients CT images: qualitative anatomical descriptions, analysis of bones curvature, and quantitative anatomical descriptions. Combinations of these approaches result in new automatic detection algorithms. Each algorithm exploits anatomical peculiarities of each attachment site, e.g., bone curvature and number of other attachments in a neighborhood of the site.

Results The experimental dataset consisted of 26 anonymized CT sequences containing right and left knee joints in different resolutions. The proposed algorithms take into account bone surface curvatures and spatial differences in locations of medial and lateral parts of both knees. The algorithms for detection of quadriceps femoris, popliteus, biceps femoris tendons, and lateral collateral and medial collateral ligaments attachment sites are provided, as well as examples of their application. Two algorithms are validated by comparison with known statistics of ligaments lengths and also using ground truth annotations for anatomical landmarks approved by clinical experts.

Conclusions The algorithms simplify generation of patient-specific knee joint models demanded in personalized biomechanical models. The algorithms in the current implementation have two important limitations. First, the correctness of the produced results depends on the bones segmentation quality. Second, the presented algorithms detect a point of the attachment site, which is not necessarily its center. Therefore, manual correction of the attachment site location may be required for attachments with relatively large area.

Keywords Knee joint · Personalized knee model · CT processing · Ligaments

Introduction

Human knee is a joint most commonly affected by activity-related injuries and joint disorders, e.g., osteoarthritis, knee bursitis, which cause pain and movement restrictions. Currently a large number of early intervention and lasting treatment techniques are developed. The development process includes testing stage which cannot always be conducted directly in vivo or can be risky for patient's health. Some experiments are carried out on cadaveric knee specimens, but their scenarios have certain restrictions. Moreover, in most of the cases prediction of treatment effects should be

✉ Alexandra Yurova
alexandra.yurova@gmail.com

Victoria Salamatova
salamatova@gmail.com

Alexey Lychagin
dr.lychagin@mail.ru

Yuri Vassilevski
yuri.vassilevski@gmail.com

[1] Sechenov University, 8-2 Trubetskaya, Moscow, Russia 119991

[2] Marchuk Institute of Numerical Mathematics RAS, 8 Gubkin Str., Moscow, Russia 119333

Published online: 13 November 2021

patient-specific, i.e., take into account individual anatomical peculiarities.

The present paper aims to describe some approaches to automatic detection of ligaments and tendons attachments sites and to present examples of the algorithms. Section 2 gives an overview of the methods developed for segmentation of anatomical structures of the knee joint. Section 3 describes input data. Three general approaches to identification of tendons and ligaments attachments are presented in section "Three general approaches to detection of tendons and ligaments attachment sites". Main algorithms for attachment sites detection are introduced in section "Algorithms for automatic detection of attachment sites", and applications of these algorithms are presented in section "Results". Discussion and conclusion constitute the final section.

Previous work

In order to evaluate parameters of interest of the knee joint, such as joint loads or contact forces, one can use biomechanical models of the human knee. Different types of knee models are known [22], and all of them require information about knee geometry.

One of the protocols for building patient-specific model of the knee joint from CT and MRI scans is presented in [21]. The model includes 21 anatomical structures and was created by semi-automatic slice-wise processing of CT and MRI datasets. The generation process is very time-consuming and can be performed only by a specialist in anatomy and radiology.

The key point in reconstruction of knee geometry is fast and accurate segmentation of multiple anatomical structures of the knee: bones and soft tissues (muscles, tendons, ligaments, cartilages).

Some algorithms for automatic segmentation of bones from CT and MRI images were introduced in [5,6,11]. In the study [1], we presented an algorithm for bones segmentation which does not require reference images (atlases) or training datasets segmented by experts. This algorithm was used for assessment of knee ligament tensions [2] by OpenSim software [4].

Automatic segmentation of soft tissues remains a challenging task because of different reasons. For instance, automatic muscles segmentation is complicated, because boundaries between them cannot be easily defined neither on CT, nor on MRI scans. In certain types of MRI sequences, intermuscular fat tissue is highlighted; however, this is not always helpful: some regions contain little amount of intermuscular fat. Moreover, muscles change shape during joints movement, which makes the reconstruction of their geometry from medical images too sophisticated. In some studies, the complex muscle geometry is represented, but the muscles were segmented manually [14].

Cartilage segmentation is used for osteoarthritis detection and also for the representation of the cartilage geometry in knee joint models. The thickness of cartilage can be less than one millimeter, and its MRI image is inhomogeneous [7]. Despite of low contrast between cartilage and adjacent structures, several approaches to its semi-automatic and automatic segmentation have been suggested in [8–10].

Representation of ligaments and tendons in biomechanical models is important, since they are involved in force transmission from muscles to bones. Tendons and ligaments can be often clearly visualized on MRI scans; however, their automatic segmentation is cumbersome due to inhomogeneity of these structures on MRI images and similarity of adjacent structures intensities. They are also hard to distinguish from surrounding soft tissues on CT scans. Algorithms for automatic or semi-automatic segmentation of anterior and posterior cruciate ligaments have been proposed in [16–18]. To the best of our knowledge, the algorithms for automatic segmentation of other ligaments and tendons are still not developed.

Thus, segmentation of knee joint medical images is not automated yet. Traditional models contain some simplifications: muscles are presented as line segments, and the patches of their attachment to bones are reduced to points [15]. Algorithms for detection of ligaments and tendons attachments sites on medical images are in great demand. A few studies address this problem. The study [12] uses statistical shape models to reconstruct ligament and tendon attachment sites in terms of contours on a 3D bone surface recovered from patient's CT scans. The method was evaluated for four ligaments (ACL, PCL, MCL and LCL): the algorithm still requires further improvements in gray value analysis and image modalities with better contrast. In [13], bone geometric models with manually detected muscles attachment sites are transformed to fit bones models of the patient. Correlation between the shape of the muscles attachment sites and the shape of the geometric models of the bones was detected, but this hypothesis was validated on the shoulder bones only.

Input data

A representation of the knee geometry is necessary to produce a plausible knee model. The crucial problem in generation of patient-specific computational models is extraction of anatomical information from medical images. For knee joint examination, both magnetic resonance imaging (MRI) and computed tomography (CT) are used [19,20,23]. MRI provides excellent soft tissue contrast and is therefore preferred for soft tissue visualization, e.g., muscles, ligaments, tendons, cartilages. CT is more suitable for imaging of cor-

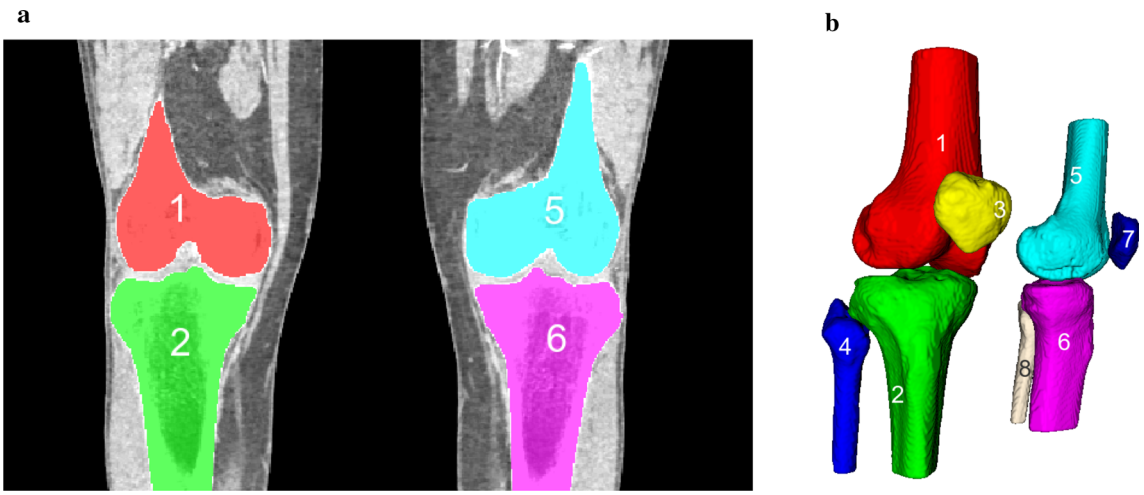

Fig. 1 Segmentation of knee CT: coronal slice (**a**), 3D view (**b**); labels: background 0, right femur 1, right tibia 2, right patella 3, right fibula 4, left femur 5, left tibia 6, left patella 7, left fibula 8

tical bones and soft tissue calcifications. Commonly several image modalities are needed to create a geometrical model of high complexity [21]. A geometric model presented in [1,2] contains attachment sites of several ligaments and tendons recovered from CT images. The present study follows this CT-based strategy and provides algorithms for detection of other ligaments and tendons attachment sites.

The experimental dataset consists of 26 anonymized CT sequences provided by Sechenov University. Each sequence contains right and left knee joints. The algorithms take into account spatial differences in locations of medial and lateral parts of both knees. The spatial dimensions are $512 \times 512 \times z$, where $z \approx 300$. The dataset can be subdivided in two subsets: 13 images have a higher resolution (voxel spacing over each axis is 0.7–0.9 mm) and 13 images have a lower resolution (voxel spacing over each axis is 1.0–1.4 mm). Application of the algorithm described in [1] results in the following labels of anatomical structures: background 0, right femur 1, right tibia 2, right patella 3, right fibula 4, left femur 5, left tibia 6, left patella 7, left fibula 8, see Fig. 1. Segmentation results serve as input data for detection of tendons and ligaments attachment sites.

All algorithms described in the paper were tested on 52 CT images of the knee joint.

Three general approaches to detection of tendons and ligaments attachment sites

Distinguishing of ligaments and tendons from adjacent soft tissues in the CT scans is complicated due to lack of soft tissue contrast. One of the goals of this study is to find characteristic anatomical features for automatic selection of points corresponding to ligaments and tendons attachment sites on the patient's bone surface. Our algorithms exploit several approaches to the solution of this problem.

Qualitative anatomical descriptions

Qualitative description of knee joint anatomy [25,26] may be used in algorithms for automatic detection of certain attachment sites, since such description implies the unique choice of their position. Section "Quadriceps femoris" presents an algorithm for detection of quadriceps femoris insertion based on qualitative anatomical description.

This and other similar algorithms possess two potential drawbacks. First, the description may be not specific enough and imply a region instead of a point. In this case, one can observe differences in illustrative materials from different sources. Second, the description is specific enough, but automatic selection of a point on the bone surface is not easy, since no particular features of the attachment location are given, e.g., "bone apex." Additional information has to be taken into account to specify peculiarities of attachment location.

Analysis of bone surface curvature

Grooves (fossae) and tubercles on bone surfaces often serve as attachment sites for ligaments and tendons and therefore can be used as landmarks in automatic detection algorithms. We consider at each point of a bone surface the Gaussian curvature which is the product of the principal curvatures $K = \kappa_1 \cdot \kappa_2$ and can be used as a surface characteristic. In particular, the Gaussian curvature of tubercles and grooves is positive. The main steps of the algorithm are as follows:

1. Generation of a bone surface mesh;
2. Computation of the surface curvature;

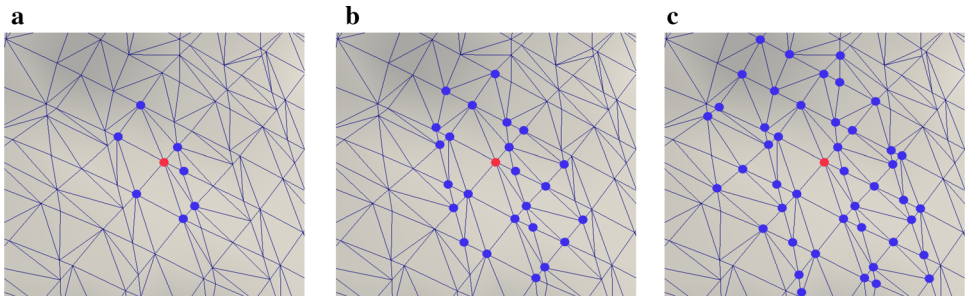

Fig. 2 r-neighborhoods of red point: $r = 1$ (**a**), $r = 2$ (**b**), $r = 3$ (**c**)

3. Selection of local maxima of the Gaussian curvature.

The first step is not performed fully automatically. A surface mesh is generated in the interface of ITK SNAP on the basis of voxel models of the bones. The obtained surface mesh is improved with Paraview Triangle filter. The C++ library Trimesh2 [33] is used to compute the principal curvatures κ_1, κ_2 of the surface patch at each point of the triangular surface mesh. A smoothing parameter is required on input. It defines the size of the mesh neighborhood where the values of the principal curvatures will be averaged after their computation. In order to distinguish grooves and tubercles, the mean curvature $H = \frac{1}{2}(\kappa_1 + \kappa_2)$ is considered: if $H < 0$, then the point is located in a groove, if $H > 0$, it is located in a tubercle. The following algorithm is used for detection of grooves or tubercles of a bone:

1. The principal curvatures are computed at each point of the mesh;
2. For each point P_i of the mesh, its r-neighborhood is searched: the set of points with graph distance less or equal r (Fig. 2);
3. If the Gaussian curvature K at point P_i achieves its maximal value in the r-neighborhood, P_i is considered to belong to a tubercle ($H > 0$) or to a groove ($H < 0$).

The choice of the algorithm parameters has been done empirically for every attachment. The parameters (the tubercle/groove size, its location and the number of other tubercles/grooves in its neighborhood) have to be taken into account in the algorithm for their automatic detection. The neighborhood size r was determined as the number of edges (graph distance), i.e., it is defined only approximately, to consider the Gaussian curvature locally. The present parameter values for r have been chosen for meshes with the edge size up to 1.5 mm. Examples of attachment sites detection based on the curvature analysis are presented in sections "Popliteus", "Biceps femoris", "Lateral collateral ligament (LCL), insertion".

Quantitative anatomical descriptions

The approaches proposed in sections "Qualitative anatomical descriptions", "Analysis of bone surface curvature" require a detailed knowledge about locations of attachment sites. Descriptions and illustrations of complex attachments are often simplified in the literature and may be different in different sources, e.g., refer to structures of medial part of the knee [30]. The assessment of such attachments is complicated.

A number of studies have performed quantitative evaluation of various anatomical structures and determined morphological landmarks in the knee joint [27–31] based on cadaveric human knees or knee radiographs. The quantitative knowledge on anatomy is useful for automatic detection of ligaments attachments sites. The examples are presented in section "Medial collateral ligament (MCL), origin".

Algorithms for automatic detection of attachment sites

Quadriceps femoris

Quadriceps femoris consists of four separate muscles attaching to the upper part of patella (Figure 3a). We exploit the fact that the intensity of quadriceps femoris tendon on CT images is higher than the intensity of other structures adjoint to the upper part of patella (Figure 3b). This fact results in the following

Algorithm 1

1. Cut the CT image into cubes composed of $3 \times 3 \times 3$ voxels and assign to each voxel the mean intensity value in the cube centered at the voxel.
2. Select patella voxels according to its label in the segmented image.
3. Dilate patella and find voxels with maximum $z_{\max}$ and minimum $z_{\min}$ z-coordinates.
4. Find a voxel v with maximum intensity value among voxels with $z \in [z_{\max} - \frac{1}{6}d; z_{\max}]$, where $d = z_{\max} - z_{\min}$.

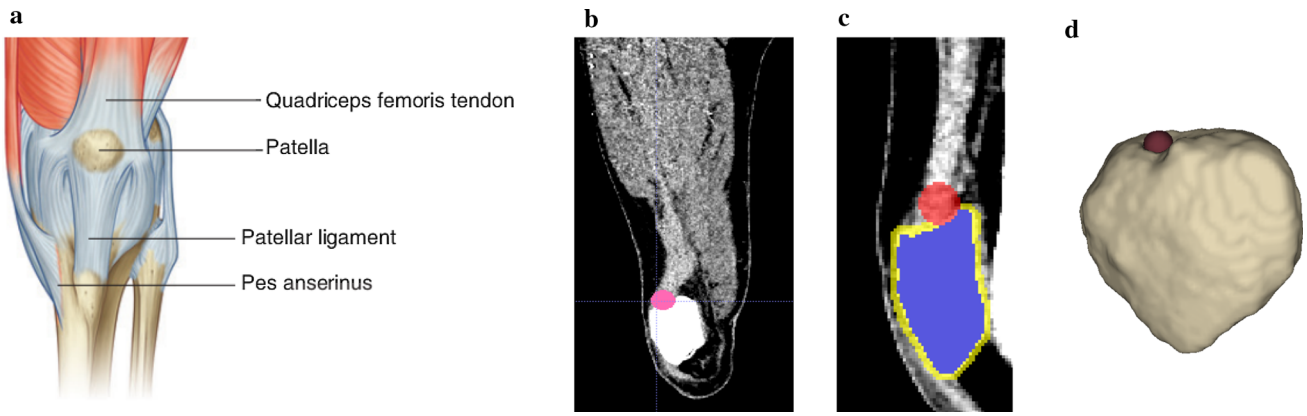

Fig. 3 Anterior view of the knee joint. Figure from [25] (**a**). The attachment of quadriceps femoris tendon to patella is marked with a pink point (**b**). Patella (blue); voxels, appeared after dilation of patella, search area for quadriceps femoris insertion (yellow); quadriceps femoris insertion (red) (**c**). The attachment of biceps femoris to patella (3D view) (**d**)

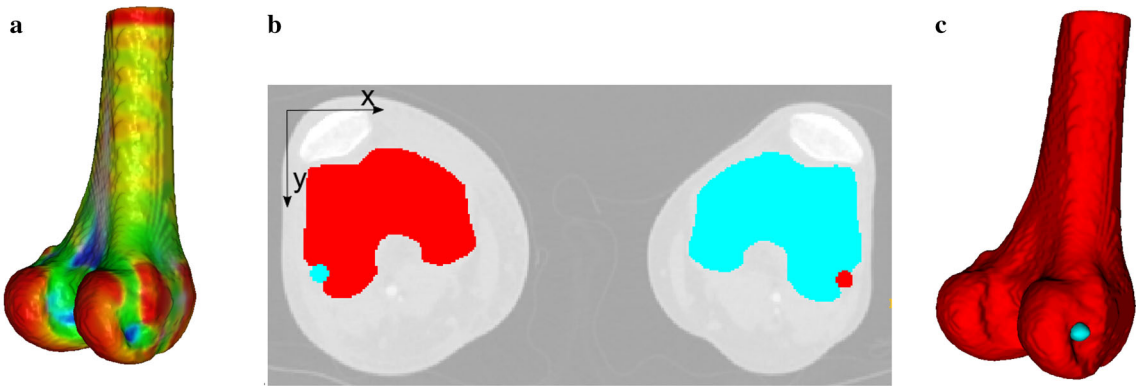

Fig. 4 Results of femur surface curvature computation (**a**). Selection of points with maximum $x + y$ value (or $x_{\max} - x + y$), depending on the bone (2D view) (**b**). Results of popliteus detection (**c**)

Popliteus

Popliteus muscle originates from the anterior part of the popliteal groove on the lateral surface of the femoral condyle. This fact is used in the algorithm for popliteus origin detection.

Algorithm 2

1. Compute curvature of the femurs surface with smoothing parameter equal to 4 (Fig. 4a).
2. Select voxels with minimum mean curvatures values in their neighborhood of radius 15.
3. Choose from the selected voxels the one with maximum $x + y$ or $x_{\max} - x + y$ value, depending on the left/right bone, see Fig. 4b–c.

Biceps femoris

The site of biceps femoris attachment is shown in Fig. 5a. The algorithm finds local maxima of the fibula surface curvature and selects the maximum having the second largest z-coordinate.

Algorithm 3

1. Compute curvatures of the fibula surface with smoothing parameter equal to 4.
2. Find all voxels which have maximum curvature value in their neighborhood of radius 15.
3. Select the voxel with the second largest z-coordinate value.

Lateral collateral ligament (LCL), insertion

LCL inserts into a depression (fossa) on the lateral surface of the fibular head (Fig. 5). The algorithm for detection of the LCL insertion is similar to Algorithm 3:

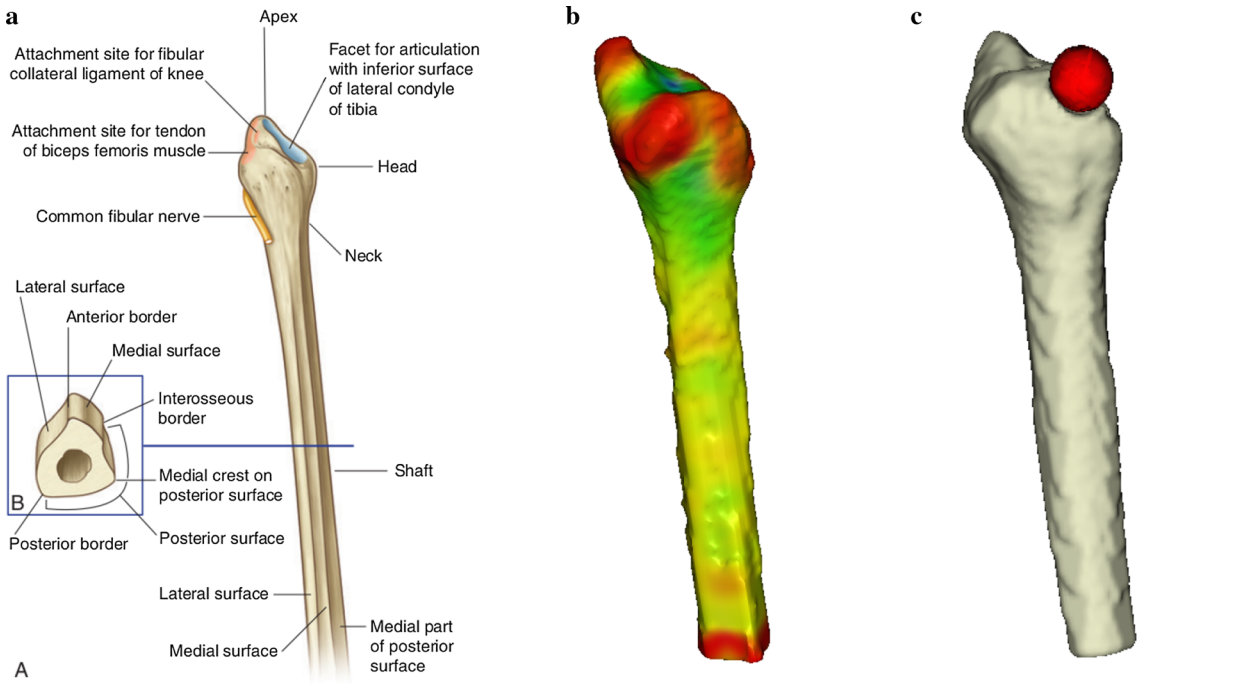

Fig. 5 Insertion of biceps femoris tendon (Image source [25]) (**a**). Results of curvature computation for fibula (**b**). Detected insertion of biceps femoris tendon (**c**)

Algorithm 4

1. Compute curvatures of the fibula surface with smoothing parameter equal to 4.
2. Find all voxels which have minimum mean curvature value in their neighborhood of radius 20.
3. Select the voxel with the largest z-coordinate value.

Medial collateral ligament (MCL), origin

MCL is attached to the femoral epicondyle, just below the adductor tubercle. Since the femoral epicondyle is a rounded eminence on the bone, one can detect it computing the bone curvature with appropriate parameters and searching its local maxima. The main difficulty is to distinguish the point located on the femoral epicondyle from the set of all local maxima (Fig. 6a). To solve this problem, we use the ratio of the femoral width and the distance from the adductor tubercle to the joint line [31]. The main knee features used for computation are shown in Fig. 6b: the joint line (JL) is the line passing through the most distal points of the medial and lateral femoral condyles in the coronal plane, ATJL is the distance between the adductor tubercle and the joint line, FW is the femoral width. According to [31], there exists simple correlation between FW and ATJL: average ATJL/FW ratio equals to 0.543. The main steps of the algorithm for detection of MCL origin are as follows.

Algorithm 5

1. Find JL and its upwards unit normal $\mathbf{n}$.
2. Compute FW and vector $\mathbf{v} = \mathbf{n} \cdot \mathrm{FW} \cdot 0.543$.
3. Add $\mathbf{v}$ to the most distal point of the medial epicondyle to obtain an approximate position of the adductor tubercle $\tilde{a}$.
4. Compute curvature of the femurs surface with smoothing parameter equal to 8.
5. Select points with maximum mean curvature values in their neighborhood of radius 5.
6. Select the closest point to $\tilde{a}$.

Results

The test dataset consists of 26 CT anonymous datasets (52 knee joints) in different resolutions provided by Sechenov University. Each joint is labeled by Nl or Nr where N is the patient number and l/r denotes left/right knee. Algorithms 1-5 are applied to each joint in order to detect the attachment sites reduced to individual voxels of the CT images. In Figs. 7, 8, 9, 10 and 11, we show the detected attachment sites for joints 3l, 5l, 6r, and 9r on the dataset with higher resolution. These joints represent (approximately) the largest or smallest lengths of ACL, PCL, LCL, and PL, rf. Table 1. Inspection of the origins or insertions presented in the figures shows correct performance of the algorithms.

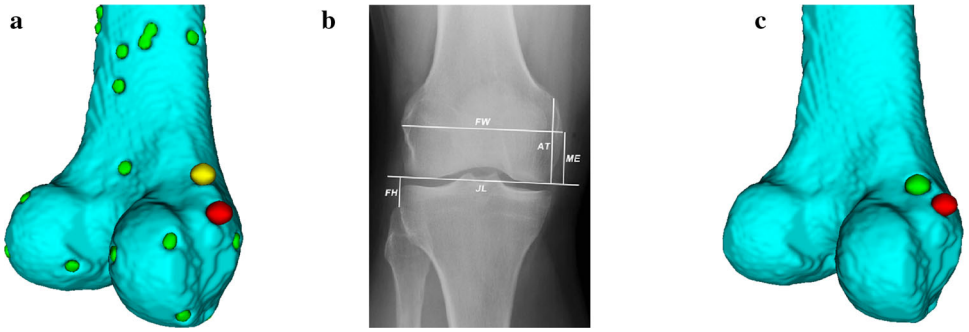

Fig. 6 Local maxima of femurs surface curvature: yellow point corresponds to adductor tubercle; red point indicates origin of MCL (**a**). An antero-posterior plain radiograph of the knee showing technique of joint measurements: ATJL (adductor tubercle to joint line), FW (femur width), FJL (fibula to joint line), JL (joint line), MEJL (medial epicondyle to joint line), Figure from [31] (**b**). Green point is the adductor tubercle according to the ratio ATJL/FW [31]; red point is the computed position of MCL origin (**c**)

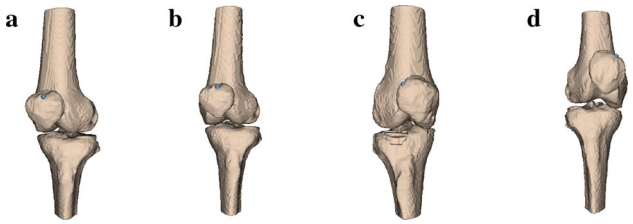

Fig. 7 Detected insertion of quadriceps femoris for joint 3l (**a**), 5l (**b**), 6r (**c**), and 9r (**d**)

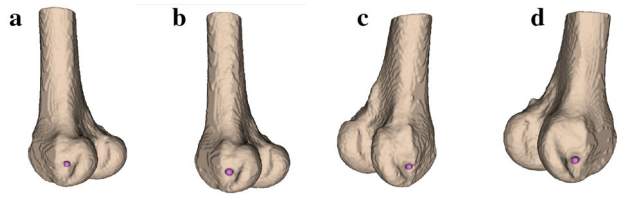

Fig. 8 Detected origins of popliteus for joint 3l (**a**), 5l (**b**), 6r (**c**), and 9r (**d**)

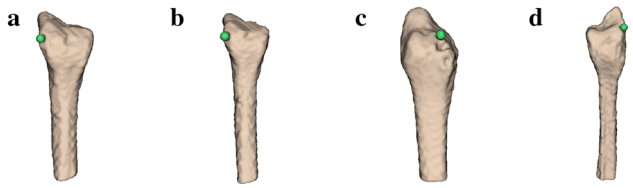

Fig. 9 Detected insertions of biceps femoris tendon for joint 3l (**a**), 5l (**b**), 6r (**c**), and 9r (**d**)

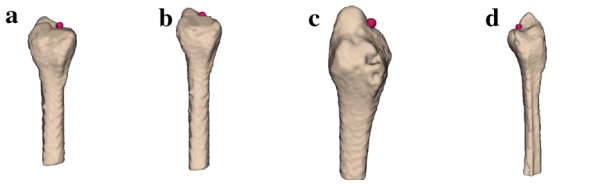

Fig. 10 Detected insertions of LCL for joint 3l (**a**), 5l (**b**), 6r (**c**), and 9r (**d**)

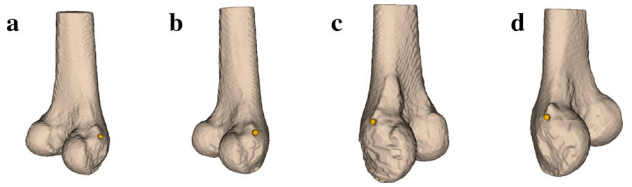

Fig. 11 Detected origins of MCL for joint 3l (**a**), 5l (**b**), 6r (**c**), and 9r (**d**)

In order to validate our algorithms, we compare statistical characteristics of certain ligaments derived in our study with those found in the literature. The statistical results for measurements of ACL, PCL, LCL, and PL lengths for 30 patients [34] are used for the validation. The attachment points for each knee were defined as mean of two–four extreme locations on the periphery of the attachment site (the most anterior, posterior, medial, lateral, distal and proximal). Table 1 contains lengths of ACL, PCL, LCL and PL (in terms of the distance between ligament origin and insertion) computed from the higher resolution CT images of 26 joints provided by Sechenov University. The length of each structure was computed as $L = \sqrt{(x_o - x_i)^2 + (y_o - y_i)^2 + (z_o - z_i)^2}$, where (x_o, y_o, z_o) and (x_i, y_i, z_i) are Cartesian coordinates of the origin and the insertion. If the coordinates of attachment sites are calculated in voxels, e.g., as in Algorithm 1, they are converted into Cartesian coordinates: $(x, y, z) = (v_x s_x + o_x, v_y s_y + o_y, v_z s_z + o_z)$, where (v_x, v_y, v_z) are voxel coordinates, (s_x, s_y, s_z) is voxel spacing, and (o_x, o_y, o_z) are the image origin coordinates.

The statistics for the lengths is compared to the statistics [34] for lower and higher resolution datasets in Tables 2, 4, respectively.

The mean length for ACL, PCL, PL derived from landmarks due to Algorithms 4–5 from data with higher resolution well correlates with that presented in [34]. The standard deviations are comparable for ACL, PCL, and LCL, whereas for PL the standard deviation is two-fold in our case. The

Table 1 Measured lengths of ACL, PCL, PL, and LCL for higher resolution datasets

Knee	ACL, mm	PCL, mm	PL, mm	LCL, mm
1r	32.288	33.247	63.985	49.555
1l	30.798	27.928	65.417	46.511
2r	31.669	37.154	65.042	43.557
2l	30.998	37.013	65.807	41.846
3r	32.288	33.138	63.983	49.118
3l	30.797	27.928	65.416	46.945
4r	32.346	33.128	63.985	49.555
4l	30.798	27.928	65.417	46.783
5r	30.211	34.477	60.436	43.665
5l	29.548	35.356	67.644	46.102
6r	33.487	28.101	54.897	49.849
6l	28.956	26.158	53.662	52.519
7r	32.424	32.489	79.91	51.788
7l	34.475	25.244	79.297	52.133
8r	31.203	38.831	79.356	50.875
8l	31.497	42.049	84.033	50.644
9r	32.424	32.489	79.91	51.788
9l	33.345	28.76	54.994	52.133
10r	46.839	52.155	83.579	51.98
10l	34.827	30.968	86.772	52.06
11r	21.886	28.074	65.568	38.679
11l	23.006	21.256	63.215	45.851
12r	32.389	33.373	53.889	36.016
12l	30.14	26.629	52.065	41.746
13r	31.577	25.518	48.734	37.816
13l	26.893	32.575	48.209	49.055

Table 2 Comparison of ACL, PCL, PL, LCL statistical characteristics (mean value, standard deviation SD, minimum and maximum values) derived from landmarks due to Algorithms 4–5 and statistics from [34] for higher-resolution dataset

Data	Mean, mm	SD, mm	Min, mm	Max, mm
ACL [34]	30.837	4.355	23.6	42.6
ACL measured	31.427	4.328	21.886	46.839
PCL [34]	31.247	4.865	21.7	40.4
PCL measured	31.999	6.286	21.256	52.155
PL [34]	63.907	5.973	54.5	76.7
PL measured	68.585	14.403	48.209	86.772
LCL [34]	58.757	5.081	46.3	67.4
LCL measured	47.253	4.857	36.016	52.519

Table 3 Measured lengths of ACL, PCL, PL, and LCL for lower resolution datasets; "—" denotes incorrect result

Knee	ACL, mm	PCL, mm	PL, mm	LCL, mm
1r	31.154	37.788	62.398	41.864
1l	29.459	35.756	68.836	48.472
2r	28.802	37.363	64.385	40.096
2l	26.556	33.543	—	40.043
3r	37.892	44.727	66.836	53.868
3l	37.554	41.903	86.105	56.112
4r	27.033	35.422	—	42.9
4l	29.373	35.779	68.847	38.743
5r	27.823	39.159	63.117	40.509
5l	28.333	34.723	66.372	38.033
6r	37.616	35.147	73.956	59.376
6l	43.009	41.155	69.309	110.355
7r	31.139	31.768	—	63.149
7l	43.648	37.308	—	—
8r	39.994	55.396	—	57.415
8l	32.704	44.944	—	83.525
9r	39.346	43.461	—	61.961
9l	43.189	38.62	69.763	—
10r	36.998	36.759	—	87.088
10l	63.074	45.264	81.191	65.421
11r	28.855	32.284	—	49.413
11l	33.973	28.291	—	99.101
12r	33.572	40.326	68.881	97.56
12l	38.676	37.402	65.6	94.361
13r	37.196	33.279	65.678	49.948
13l	55.249	49.791	41.911	48.453

Table 4 Comparison of ACL,PCL,PL,LCL statistical characteristics (mean value, standard deviation SD, minimum and maximum values) derived from landmarks due to Algorithms 4-5 and statistics from [34] for lower-resolution dataset

Data	Mean, mm	SD, mm	Min, mm	Max, mm
ACL [34]	30.837	4.355	23.6	42.6
ACL measured	36.239	8.624	26.556	63.074
PCL [34]	31.247	4.865	21.7	40.4
PCL measured	38.745	5.939	28.291	55.396
PL [34]	63.907	5.973	54.5	76.7
PL measured	67.699	9.334	41.911	86.105
LCL [34]	58.757	5.081	46.3	67.4
LCL measured	53.319	13.968	38.033	87.088

mean length of LCL reported in [34] is 11 mm larger than the mean length of LCL based on the landmarks due to Algorithms 4–5, although the standard deviations are comparable. This indicates to a systematic discrepancy of the measurements due to different definitions of LCL length. We measure the distance between voxel (pointwise) landmarks of insertions and origins, whereas one may include the attachment region size to the length of the ligament. According to [35], the average cross-sectional area of the fibular collateral ligament attachment site on the femur was 0.48 cm^2 (ranging

from 0.43 to 0.52); the average cross-sectional area of the attachment on the fibular head was 0.43 cm^2 (ranging from 0.39 to 0.50). The 11mm discrepancy may be caused by differences in the attachment point location within the attachment area.

The experiments with lower resolution datasets were also carried out. The difference of the mean length and that presented in [34] is greater compared to the case of higher resolution dataset. The algorithms based on the curvature analysis are sensitive to data resolution and may even produce incorrect results (Table 3), since local curvature recovery for lower-resolution datasets may be prone to large numerical errors. A large number of incorrect results for PL are caused by the wrong tibial tuberosity detection. Parameter tuning for this algorithm is required (Table 4).

The accuracy of the segmentation results for higher resolution was also evaluated using ground truth annotations provided by clinical experts. The distance errors were measured for 208 points: origins and insertions of ACL, PCL, PL, and LCL ligaments for 26 knee joints (13 datasets). The mean error for all points is 12mm; the maximal error is 23 mm. The biggest error values were achieved for attachments with relatively large area, e.g., ACL, PCL, PL. The length of the femoral ACL attachment was 17.9 ± 2.0 mm (mean$\pm$ SD) [37]; the femoral attachment of the PCL extends more than 20 mm in an anterior-posterior direction [38]. For these attachments, the error depends on the point selection within the attachment area.

Discussion and conclusion

We discussed three approaches to automatic detection of tendons and ligaments attachment sites. The approaches are based on the qualitative and quantitative anatomical descriptions as well as analysis of the bone surface curvature. The examples of the detection algorithms based on these approaches were presented. The algorithms were tested on knee CT images of 26 anonymous patients. The detected sites were approved by experienced clinicians. The statistics for ACL, PCL, PL, LCL lengths due to Algorithms 4 and 5 was compared to the statistics reported in [34]. The detected attachments of ACL, PCL, PL, LCL were compared with ground truth annotations provided by clinical experts for 13 CT images (26 knee images) in higher resolution. The other algorithms cannot be validated in the similar way since the considered ligament/tendon has origin or insertion located outside the knee joint.

Since some of the proposed algorithms are based on the local curvature properties of the bones surface, the correctness of the segmentation depends on the bones segmentation quality. Most of the segmentation methods take into account (in some form) significantly higher intensity values of the bones cortical layer in comparison with surrounding tissues. Thinning of the cortical layer is common in the case of older patients. If the cortical layer thickness is comparable to CT voxel spacing, the bone boundary cannot be detected correctly and manual segmentation correction is required. It is crucial for local neighborhoods of the attachments sites. Manual correction of the femur boundaries was carried out for several patients in order to obtain accurate attachment sites.

For datasets with higher resolution, the measured mean lengths for ACL, PCL, PL well match to the statistics [34]. The measured mean length for LCL is 11 mm smaller in our case due to different definitions of the LCL length. The systematic discrepancy is caused by possible inclusion of fractions of the attachment sizes to the LCL length in [34]. For datasets with lower resolution, the matching with statistics [34] is worse. To obtain better results for the lower resolution images, some parameters of the algorithms need to be adjusted.

Ligaments and tendons attachment sites may be used as anatomical landmarks for registration purposes and in the development of personalized biomechanical models.

Funding The research was funded by Russian Science Foundation grant 21-71-30023.

Declarations

Conflict of interest The authors declare that they have no conflict of interest.

Ethics approval The data were obtained retrospectively from anonymized databases and not generated intentionally for the study. For this type of study, a formal consent is not required.

Informed consent There is no informed consent required for the work reported in this manuscript.

References

1. Salamatova VY, Yurova AS, Vassilevski YV, Wang L (2019) Automatic segmentation algorithms and personalized geometric modelling for a human knee. Russ J Numer Anal Math Model 34(6):361–367. https://doi.org/10.1515/rnam-2019-0031
2. Yurova A, Salamatova V, Vassilevski Y, Wang L, Goreynov S, Kosukhin O, Shipilov A, Aliev Y (2021) Personalized geometric modeling of a human knee: data, algorithms, outcomes. In: Favorskaya MN, Favorskaya AV, Petrov IB, Jain LC(eds) Smart modelling for engineering systems, smart innovation, systems and technologies, vol 214. Springer. https://doi.org/10.1007/978-981-33-4709-0_18
3. CGAL 5.3 - Surface Mesh https://doc.cgal.org/latest/Surface_mesh/index.html
4. Free project-hosting platform for the biomedical computation community https://simtk.org
5. Wu D, Sofka M, Birkbeck N, Zhou SK (2014) Segmentation of Multiple Knee Bones from CT for Orthopedic Knee Surgery Plan-

ning. In: Golland P, Hata N, Barillot C, Hornegger J, Howe R (eds) Medical image computing and computer-assisted intervention - MICCAI 2014. MICCAI 2014. Lecture Notes in Computer Science, vol 8673. Springer, Cham
6. Fripp J, Warfield SK, Crozier S, Ourselin S (2006) Automatic segmentation of the knee bones using 3D active shape models. In: 18th international conference on pattern recognition (ICPR'06), Hong Kong, pp 167–170. https://doi.org/10.1109/ICPR.2006.306
7. Vilimek D, Kubíček J, Penhaker M, Oczka D, Augustynek M, Cerny M (2019) Current automatic methods for knee cartilage segmentation: a review. https://doi.org/10.1109/EUVIP47703.2019.8946132
8. Iranpour-Boroujeni T, Watanabe A, Bashtar R, Yoshioka H, Duryea J (2011) Quantification of car-tilage loss in local regions of knee joints using semi-automated segmentation software: analysis of longitu-dinal data from the Osteoarthritis Initiative (OAI). Osteoarthritis and Cartilage 19(3):309–314
9. Folkesson J, Dam E, Olsen O, Pettersen P, Christiansen C (2007) Segmenting articular cartilage automatically using a voxel classification approach. IEEE Trans Med Imaging 26:106–115. https://doi.org/10.1109/TMI.2006.886808
10. Fripp J, Crozier S, Warfield SK, Ourselin S (2010) Automatic segmentation and quantitative analysis of the articular cartilages from magnetic resonance images of the knee. IEEE Trans Med Imaging 29(1):55–64. https://doi.org/10.1109/TMI.2009.2024743
11. Ambellan F, Tack A, Ehlke M, Zachow S (2019) Automated segmentation of knee bone and cartilage combining statistical shape knowledge and convolutional neural networks: Data from the Osteoarthritis Initiative. Med Image Anal 52:109–118
12. Seim H, Lamecker H, Heller M, Zachow S (2008) Segmentation of bony structures with ligament attachment sites. Informatik aktuell. https://doi.org/10.1007/978-3-540-78640-5_42
13. Kaptein B, van der Helm F (2004) Estimating muscle attachment contours by transforming geometrical bone models. J Biomech 37:263–73. https://doi.org/10.1016/j.jbiomech.2003.08.005
14. Delp S, Blemker S (2005) Three-dimensional representation of complex muscle architectures and geometries. Ann Biomed Eng 33:661–73. https://doi.org/10.1007/s10439-005-1433-7
15. Blemker SS, Asakawa DS, Gold GE, Delp SL (2007) Image-based musculoskeletal modeling: applications, advances, and future opportunities. J Magn Reson Imaging 25(2):441–451. https://doi.org/10.1002/jmri.20805
16. Lee H, Hong H, Kim J (2013) Anterior cruciate ligament segmentation from knee MR images using graph cuts with geometric and probabilistic shape constraints. In: Lee KM, Matsushita Y, Rehg JM, Hu Z (eds) Computer vision - ACCV 2012. ACCV 2012. Lecture Notes in Computer Science, vol 7725. Springer, Berlin, Heidelberg
17. Uozumi Y, Nagamune K, Mizuno K (2015) Computer-aided segmentation system of posterior cruciate ligament in knee joint from CT and MRI using anatomical information: A Pilot Study of System Configuration. In: 2015 IEEE international conference on systems, man, and cybernetics, Kowloon, pp 2295–2298. https://doi.org/10.1109/SMC.2015.401
18. Paproki A, Wilson KJ, Surowiec RK, Ho CP, Pant A, Bourgeat P, Engstrom C, Crozier S, Fripp J (2016) Automated segmentation and T2-mapping of the posterior cruciate ligament from MRI of the knee: data from the osteoarthritis initiative. In: IEEE 13th international symposium on biomedical imaging (ISBI). Prague 2016:424–427. https://doi.org/10.1109/ISBI.2016.7493298
19. Nacey NC, Geeslin MG, Miller GW, Pierce JL (2017) Magnetic resonance imaging of the knee: An overview and update of conventional and state of the art imaging. J Magn Reson Imaging 45(5):1257–1275. https://doi.org/10.1002/jmri.25620
20. Hayashi D, Roemer FW, Guermazi A (2016) Imaging for osteoarthritis. Ann Phys Rehabil Med 59(3):161–169
21. Dong Y, Mou Z, Huang Z, Hu G, Dong Y, Xu Q (2013) Three-dimensional reconstruction of subject-specific knee joint using computed tomography and magnetic resonance imaging image data fusions. Proc Inst Mech Eng H 227(10):1083–1093. https://doi.org/10.1177/0954411913493723
22. Madeti B, Rao CS, Pragada S (2015) Biomechanics of knee joint - A review. Front Mech Eng 10:176–186. https://doi.org/10.1007/s11465-014-0306-x
23. Amano K, Li Q, Ma CB (2016) Functional knee assessment with advanced imaging. Curr Rev Musculoskelet Med 9(2):123–129. https://doi.org/10.1007/s12178-016-9340-0
24. Hofer Matthias (2010) CT Teaching Manual: A Systematic Approach to CT Reading. Thieme
25. Drake R, Vogl AW, Mitchell A (2019) Gray's Anatomy for students. 4th Edition. Elsevier
26. Prives M, Lysenkov N, Bushkovich V. (Prives M.G.,Lysenkov N.K.,Bushkovich V.I.). Human anatomy. Volume 1, Volume 2. (Anatomiya cheloveka .V 2-h tomah)
27. Saigo T, Tajima G, Kikuchi S, Yan J, Maruyama M, Sugawara A, Doita M (2017) Morphology of the insertions of the superficial medial collateral ligament and posterior oblique ligament using 3-dimensional computed tomography: a cadaveric study. Arthroscopy 33(2):400–407
28. Lee JH, Kim KJ, Jeong YG, Lee NS, Han SY, Lee CG, Kim KY, Han SH (2014) Pes anserinus and anserine bursa: anatomical study. Anatomy Cell Biol 47(2):127–131
29. Liu F, Yue B, Gadikota HR, Kozanek M, Liu W, Gill TJ, Rubash HE, Li G (2010) Morphology of the medial collateral ligament of the knee. J Orthop Surg Res 5:69. https://doi.org/10.1186/1749-799X-5-69
30. LaPrade RF, Engebretsen AH, Ly TV, Johansen S, Wentorf FA, Engebretsen L (2007) The anatomy of the medial part of the knee. J Bone Joint Surg Am 89(9):2000–2010. https://doi.org/10.2106/JBJS.F.01176
31. Iacono F, Lo Presti M, Bruni D, Raspugli GF, Bignozzi S, Sharma B, Marcacci M (2013) The adductor tubercle: a reliable landmark for analysing the level of the femorotibial joint line. Knee Surg Sports Traumatol Arthrosc 21(12):2725–9
32. Pereira G, von Kaeppler E, Alaia M, Montini K, Lopez M, Di Cesare P, Amanatullah D (2016) Calculating the position of the joint line of the knee using anatomical landmarks. Orthopedics 39:381–386. https://doi.org/10.3928/01477447-20160729-01
33. Trimesh2, C++ library and set of utilities for input, output, and basic manipulation of 3D triangle meshes
34. Clément B, Drouin G, Shorrock G, Gely P (1989) Statistical analysis of knee ligament lengths. J Biomech 22(8–9):767–774
35. LaPrade R, Ly T, Wentorf F, Engebretsen L (2003) The posterolateral attachments of the knee a qualitative and quantitative morphologic analysis of the fibular collateral ligament, Popliteus Tendon, Popliteofibular Ligament, and Lateral Gastrocnemius Tendon*. Am J Sports Med 31:854–60
36. Voos JE, Mauro CS, Wente T, Warren RF, Wickiewicz TL (2012) Posterior cruciate ligament: anatomy, biomechanics, and outcomes. Am J Sports Med 40(1):222–31
37. Kawaguchi Y, Kondo E, Takeda R, Akita K, Yasuda K, Amis AA (2015) The role of fibers in the femoral attachment of the anterior cruciate ligament in resisting tibial displacement. Arthroscopy 31(3):435–444
38. Amis AA, Gupte CM, Bull AM, Edwards A (2006) Anatomy of the posterior cruciate ligament and the meniscofemoral ligaments. Knee Surg Sports Traumatol Arthrosc 14(3):257–63